IEEE Access
Multidisciplinary ⋮ Rapid Review ⋮ Open Access Journal

Received July 22, 2020, accepted July 29, 2020, date of publication August 3, 2020, date of current version August 13, 2020.

Digital Object Identifier 10.1109/ACCESS.2020.3013570

Robust μ-Synthesis With Dahl Model Based Feedforward Compensator Design for Piezo-Actuated Micropositioning Stage

IRFAN AHMAD, MAHMOUD A. ALI, AND WONSUK KO
Department of Electrical Engineering, College of Engineering, King Saud University, Riyadh 11451, Saudi Arabia
Corresponding author: Irfan Ahmad (irfahmad@ksu.edu.sa)

This work was supported by the Deanship of Scientific Research at King Saud University through research group no. RG-1439-028.

ABSTRACT In this article, a combined feedback-feedforward control design scheme is presented to enhance the tracking performance of a piezo-actuated micropositioning stage by compensating the nonlinear hysteretic behavior of the piezoelectric actuator and model uncertainties of the system. Detailed investigation of the presented control scheme is performed not only in simulation by analyzing the robust stability and robust performance but also in real-time with motion trajectories of multiple frequencies. To design the presented control scheme, first of all, the dynamic model of the system is identified from the real-time experimental data by using the recursive least squares parameter adaptation algorithm. Then, Dahl hysteresis model is considered to represent the nonlinear hysteretic behavior of the piezoelectric actuator. To deal with this hysteresis nonlinearity, Dahl feedforward compensator is designed without involving inverse model calculations to avoid any computational complexity. This feedforward compensator is then combined with μ-synthesis robust feedback controller which is designed in the presence of model uncertainties of the system. The presented control scheme ensures the boundedness of the closed-loop signals and the desired tracking performance of the considered micropositioning stage. Finally, experimental tests are conducted with motion trajectories of multiple frequencies for the validation of the control scheme. An average improvement of 95% in compensating the hysteresis nonlinearity and 80% in reducing the tracking error is achieved which demonstrates the efficacy of the presented control scheme.

INDEX TERMS Dahl feedforward compensator, hysteresis nonlinearity, micropositioning, model uncertainties, piezoelectric actuator, μ-synthesis robust feedback controller.

I. INTRODUCTION

Over the past decades, the rapid advancements have been witnessed in the field of ultra-precise micro/nanopositioning stages. It has been widely acknowledged in the literature that the piezo-actuated micro/nanopositioning stages have remarkable advantages in terms of ultra-high positioning precision, nanometer or subnanometer resolution, large mechanical force, compact design, less power consumption and fast response time [1]. Due to these numerous advantages, piezo-actuated positioning stages are commonly used in many applications, e.g. in scanning probe microscopy [2], advanced lithography tools for the fabrication of semiconductor integrated circuits [3], servo system of hard disk-drives [4], optical alignment systems [5], manipulation of nanoscale biological process like DNA analysis [6] and also in the manufacturing of small objects [7]. In all these applications, ultra-precise positioning with high speed and long positioning range is desired. However, there are certain challenges involved in order to achieve the desired performance of the piezo-actuated positioning stages. One of these challenges comes from the inherent hysteresis and creep nonlinearities of the piezoelectric actuator. The desired performance of the piezo-actuated positioning stages suffers or even the control system may become unstable if these nonlinearities of the piezoelectric actuator are not compensated with a suitable control methodology [8]. The hysteresis nonlinearity of the piezoelectric actuator depends on the amplitude of the applied

The associate editor coordinating the review of this manuscript and approving it for publication was Tao Wang.

input voltage. The creep nonlinearity is related to the drift phenomenon of the output displacement of the piezoelectric actuator when subjected to a constant input voltage. However, the effects of creep phenomenon become noticeable only when the tracking is performed over extended periods of time during slow-speed operations. Another main challenge, particularly while working at micro or nano scale, is the change in the operating conditions, like ambient temperature, humidity etc., which introduces the uncertainty in the system model. Therefor, control design based on a single system model may not achieve the desired performance while working in real-time over an experimental platform [9]. Model uncertainty necessitates the design of a robust control methodology in order to achieve not only nominal stability and nominal performance but also robust stability and robust performance. All these challenges need to be addressed in order to achieve the desired performance of the piezo-actuated positioning stages.

Lots of research has been done in modeling and controlling of piezo-actuated positioning stages so far. A number of nonlinear models to represent hysteresis nonlinearity of piezoelectric actuator are investigated in the literature. Some of these models are differential based models, like Duhem model [10], Bouc-Wen model [11], Dahl model [12], and some models are operator based models, like Prandtl-Ishlinskii model [13], Preisach model [14], Maxwell model [15] and Krasnosel'skii-Pokrovskii model [16] etc. To compensate the hysteresis nonlinearity, two different control strategies are generally adopted in the literature. The first control strategy is to design a feedforward compensator as an inverse hysteresis model and then to cascade it with piezoelectric actuator in open-loop configuration [17]–[19]. This first control strategy has to deal with computational complexity while performing inversion of the actual hysteresis model. To avoid this computational complexity, a few approaches are presented in the literature which avoid calculating the inverse hysteresis model for the feedforward compensator [20], [21]. Real-time implementation of these feedforward compensators may not achieve the desired performance in the presence of modeling error and unknown disturbances. The second control strategy is an integrated design approach, where a feedback controller is generally combined with a feedforward compensator. Different feedback control algorithms, like fuzzy control [22], adaptive control [23], model predictive control [24], sliding mode control [25], robust and optimal control [26], [27] and classical proportional-integral-derivative control [28] are investigated in the literature in the presence of feedforward compensators. Other than these two control strategies, another approach to compensate the hysteresis nonlinearity is to use the charge-driven piezoelectric actuators [29]. However, this method needs to deal with increased hardware complexity. To deal with creep nonlinearity of the piezoelectric actuator, a number of models with control strategies [30]–[32] are discussed in the literature. However, working in closed-loop for a short interval of time suppresses the creep nonlinearity. Hence, creep compensation is not discussed in this article. Regarding performance analysis of the piezo-actuated positioning stage with model uncertainties, most of the research work in the literature is based on just a single parameter variation which is the resonant frequency of the positioning stage [33]. The most effective solution to deal with this uncertainty is to damp the resonant mode of the positioning stage with a suitable damping controller [34]. An adaptive fuzzy fractional-order nonsingular terminal sliding mode controller (AFFO-NTSMC) is investigated to analyze the tracking performance of a second-order uncertain nonlinear dynamic system [35]. The presented simulation results with AFFO-NTSMC show small tracking errors with well attenuation of the chattering phenomenon, which is very common in conventional sliding mode control algorithm, in the presence of model uncertainties. Adaptive fuzzy control is also discussed in [36]–[38] to analyze the tracking problem of the uncertain nonlinear systems. The performance of the robust H_∞ feedback controller is investigated in [39] for linear systems with polytopic uncertainties. It has been observed by the authors of this article that there is a scarcity of research work about the detailed analysis in terms of robust stability and robust performance of the piezo-actuated positioning stages in the presence of model uncertainties with hysteresis nonlinearity.

In this article, the hysteresis nonlinearity of the considered piezoelectric actuator is first modeled by considering the Dahl hysteresis model and then its compensator is designed to use it as a feedforward compensator. The Dahl feedforward compensator is designed without calculating the inverse hysteresis model to avoid any computational complexity. After linearizing the hysteresis nonlinearity with the feedforward compensator, the μ-synthesis robust feedback controller is designed, in the presence of model uncertainties of the system, to enhance the tracking performance of the considered piezo-actuated micropositioning stage. Therefore, other than closed-loop nominal stability and nominal performance of the system, robust stability and robust performance analysis is also presented in this article. The main contributions of this article are as follows:

- A combined feedback-feedforward control design scheme is presented, where the Dahl feedforward compensator is designed without formulating the inverse hysteresis model and the μ-synthesis robust feedback controller is designed in the presence of model uncertainties of the system. According to the authors' knowledge, the presented control scheme in this article has not been analyzed in the literature of micropositioning stages so far.
- Experimental validation of the system model as well as the presented control scheme with motion trajectories of multiple frequencies is also a part of this article.

The remainder of this article is organized as follows: *Section II* describes a brief description of the considered piezo-actuated micropositioning stage with all the necessary details about the experimental setup, used for the real-time validation of the model and the control scheme. Modeling of

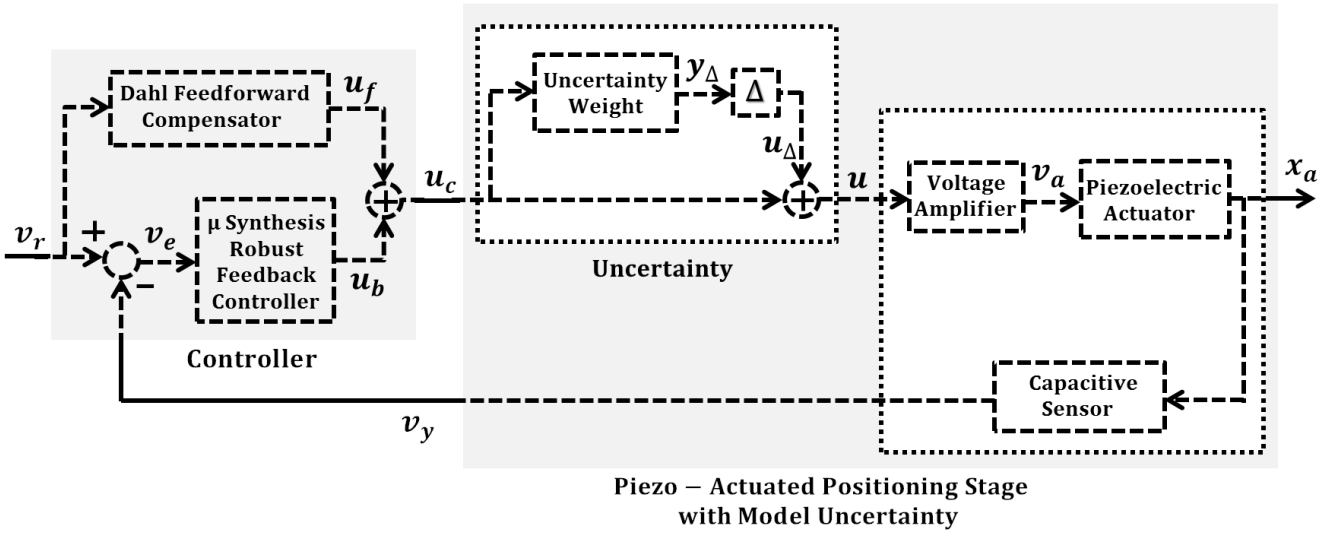

FIGURE 1. Block diagram of the piezo-actuated micropositioning system with a combined feedback-feedforward control scheme.

the piezo-actuated micropositioning system, which includes linear time-invariant (LTI) dynamic model, uncertainty model and hysteresis model, is presented in *Section III*. *Section IV* of this article deals with the controller design. Closed-loop nominal stability and nominal performance as well as robust stability and robust performance are also discussed in this section. Experimental results are thoroughly analyzed in *Section V*. Finally, concluding remarks are presented in *Section VI*.

II. DESCRIPTION OF PIEZO-ACTUATED MICROPOSITIONING STAGE

The complete block diagram of the considered piezo-actuated micropositioning system, in the presence of Dahl feedforward compensator and μ-synthesis robust feedback controller, is presented in Fig. 1. The considered micropositioning system consists of a voltage amplifier, piezoelectric actuator, capacitive position sensor, data acquisition module, and a host computer for the implementation of the control algorithm. The block diagram of the micropositioning experimental loop is presented in Fig. 2. The presented control scheme is the combination of Dahl feedforward compensator and the μ-synthesis robust feedback controller. Dahl feedforward compensator is designed to mitigate the effects of nonlinear hysteresis phenomenon of the piezoelectric actuator. The μ-synthesis robust feedback controller is designed to achieve the desired tracking performance with robustness and stability. The presented control approach ensures the boundedness of the closed-loop signals and the desired tracking performance.

The considered 1D all-ceramic insulated piezo-actuated micropositioning stage ($P-752.21$ produced by Physik Instrumente GmbH & Co.) is having an integrated capacitive displacement sensor ($D-015$). Flexure-guide based piezo-actuated positioning stage with all-ceramic insulation

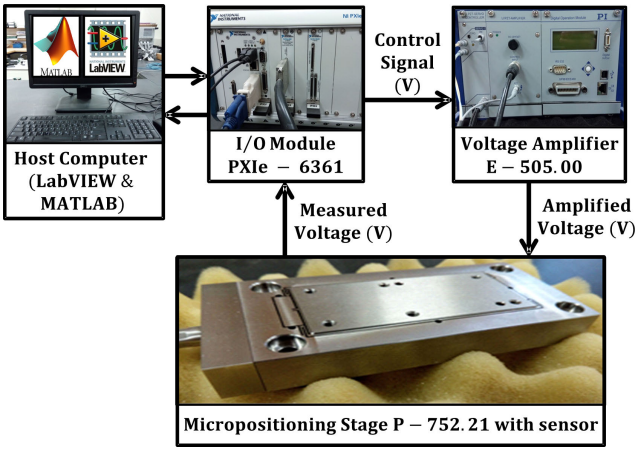

FIGURE 2. Block diagram of the experimental loop.

offers high travel accuracy, rapid response, high load capacity and longer lifetime than conventional polymer-insulated actuators. Flexure-guide based positioning stages have been widely used in different precision engineering applications from one degree of freedom to six degrees of freedom [40]–[42]. The travel range of the considered piezoelectric actuator is 35 μm with the resolution of 0.2 nm and maximum load capacity of 30 N. The specifications of the considered piezo-actuated micropositioning stage are listed in *Table 1*. The displacement (x_a) of the piezoelectric actuator is sensed by the capacitive sensor ($D-015$) which can measure with subnanometer resolution. Generally, the capacitive sensor is widely used as a displacement sensor for precise measurement with subnanometer resolution and high bandwidth. This sensor has an extended measuring range of 45 μm with a resolution of 0.01 nm. The bandwidth of this sensor is 10 kHz and the analog output voltage range is from 0 to 10 V. This analog output voltage (v_y) is given to the host computer through

TABLE 1. Properties of piezo-actuated micropositioning stage.

Items	Quantity	Units
Driven voltage	-20 to 120	V
Travel range (displacement)	0 to 35	μm
Resolution	0.2	nm
Resonant frequency	2100	Hz
Load capacity	30	N
Stiffness in motion direction	20	N/μm
Electrical capacitance	3.7	μF
Stage mass	0.35	kg

a 16-bit multi-function I/O module ($PXIe-6361$ produced by National Instruments). The host computer has LabVIEW software for the implementation of the control algorithm and MATLAB for the analysis of the achieved results.

In the host computer, the analog output voltage (v_y), given by the I/O module, is compared with the reference input voltage (v_r) in order to find the error signal (v_e). The reference input voltage (v_r) corresponds to the desired displacement of the piezo-actuated micropositioning stage. In the presented control scheme, the feedforward compensator acts on the reference voltage (v_r), whereas the feedback controller acts on the error voltage (v_e) as shown in Fig. 1. The control action of the feedforward compensator (u_f) is summed up with the control action of the feedback controller (u_b) to generate the control input (u_c). The voltage amplifier ($E-505$) receives the control input through I/O module and amplifies it with a fixed gain of 10 to derive the piezoelectric actuator. The bandwidth of the voltage amplifier is 3 kHz. The input voltage range of this amplifier is from -2 to $+12$ V and the output voltage range is from -30 to $+130$ V. The mathematical modeling of the considered piezo-actuated micropositioning stage is presented in the next section.

III. MODELING OF PIEZO-ACTUATED MICROPOSITIONING STAGE

In this section, LTI dynamic model, uncertainty model and Dahl hysteresis model of the considered piezoelectric actuator with the experimental validations are presented.

A. LINEAR-TIME-INVARIANT (LTI) DYNAMIC MODEL

The LTI dynamic model of the piezo-actuated micropositioning system is achieved from the real-time experimental data. Four main steps in order to achieve the model from the experimental data are presented in Fig. 3.

Step I: To achieve the LTI dynamic model, a sinusoidal chirp excitation signal of increasing frequency and small magnitude is applied to the piezo-actuated positioning stage in an open-loop configuration. This excitation signal has a rich frequency spectrum in order to cover the bandwidth of the system to be identified and a small magnitude to suppress the nonlinear hysteresis of the actuator.

Step II: The model complexity is selected by trial and error with six poles and three zeros. The reason for selecting the 6^{th} order LTI dynamic model for the considered piezo-actuated

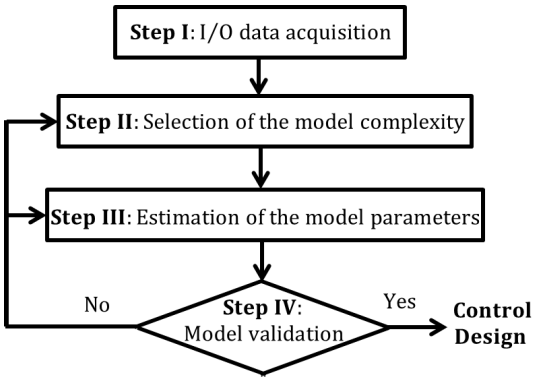

FIGURE 3. Steps for system identification.

micropositioning system is to capture the high frequency vibrations while working at high speeds.

Step III: A recursive least squares (RLS) parameter adaptation algorithm is used for estimating the parameters of the LTI dynamic model. The basic idea of this algorithm is to minimize the error (prediction error) between the experimental output and the output predicted by the model, by modifying the model parameters at each sampling instant. Due to the recursive structure of the algorithm, the new value of the estimated parameters is equal to the previous value plus a correction term that will depend on the most recent measurements. Let $\hat{\Psi}(t)$ is a vector of the estimated model parameters at time t, $\theta(t)$ is a measurement vector or plant model regressor vector at time t, then *a priori* prediction error $e^0(t+1)$ can be computed at the instant $t+1$ after the acquisition of the output measurement $y(t+1)$ as:

$$e^0(t+1) = y(t+1) - \hat{\Psi}^T(t)\,\theta(t) \tag{1}$$

Now, according to the recursive least squares parameter adaptation algorithm, the vector of estimated model parameters at the instant $t+1$ can be computed with the help of $\hat{\Psi}(t)$ plus a correction term, as:

$$\hat{\Psi}(t+1) = \hat{\Psi}(t) + W(t+1)\,\theta(t)\,e^0(t+1) \tag{2}$$

where, $W(t+1)$ is a time varying gain matrix which can be computed as:

$$W(t+1) = W(t) - \frac{W(t)\,\theta(t)\,\theta^T(t)\,W(t)}{1+\theta^T(t)\,W(t)\,\theta(t)} \tag{3}$$

Further details about the parameter adaption algorithm can be found in [43].

The achieved 6^{th} order LTI dynamic model G(s) of the considered piezo-actuated micropositioning system is given as follows:

$$G(s) = \frac{b_3 s^3 + b_2 s^2 + b_1 s + b_0}{s^6 + a_5 s^5 + a_4 s^4 + a_3 s^3 + a_2 s^2 + a_1 s + a_0} \tag{4}$$

The identified parameters of the model are: $a_0 = 2.05\times10^{23}$, $a_1 = 5.79\times10^{19}$, $a_2 = 1.65\times10^{16}$, $a_3 = 1.98\times10^{12}$,

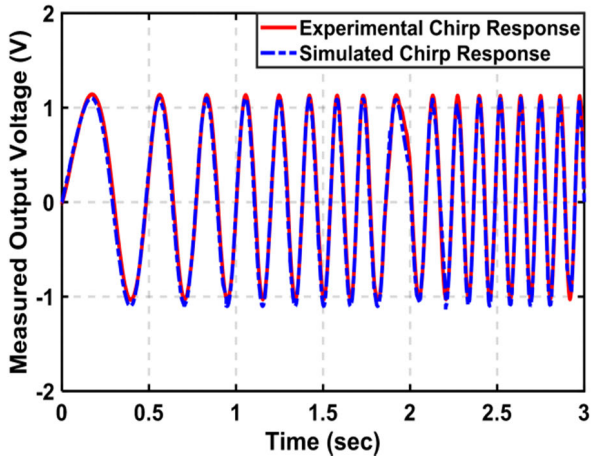

FIGURE 4. Experimental and simulated chirp responses for the validation of the LTI model.

$a_4 = 2.95 \times 10^8$, $a_5 = 1.08 \times 10^4$, $b_0 = 1.84 \times 10^{23}$, $b_1 = 2.76 \times 10^{19}$, $b_2 = 4.74 \times 10^{15}$ and $b_3 = 2.01 \times 10^{11}$.

Step IV: The identified LTI dynamic model is validated if the prediction error between the experimental output and the output predicted by the model asymptotically tends towards white noise. This will result in a close match between the simulated response of the identified model and the experimental response. The experimental and simulated chirp responses are compared in Fig. 4 for the validation of the model. A close match between these two plots validates the achieved LTI dynamic model of the considered system. A small difference between these plots can also be observed, which will be dealt with the robustness of the presented robust feedback controller in the presence of model uncertainties.

B. UNCERTAINTY MODEL

The characteristic equation of the identified LTI dynamic model is $s^6 + a_5 s^5 + a_4 s^4 + a_3 s^3 + a_2 s^2 + a_1 s + a_0 = 0$. The parameters $(a_0, a_1, \cdots, a_5)$ of this characteristic equation may vary due to changes in the operating conditions like ambient temperature, humidity, etc., which introduces the uncertainty in the system model. To account for model uncertainty, the dynamic behavior of the piezo-actuated micropositioning system is represented by a set Π of possible LTI models which are developed with the variation of $\pm 5\%$ in each parameter of the characteristic equation. By considering the input multiplicative uncertainty, the uncertain system model can be represented as:

$$G_\Delta(s) = G(s)(1 + H_m(s)\Delta(s)); \quad |\Delta(j\omega)| \leq 1, \ \forall\omega \tag{5}$$

where, $G \in \Pi$ is a nominal plant model, $G_\Delta \in \Pi$ uncertain plant model, H_m multiplicative uncertainty weighting function and Δ is any stable transfer function, satisfying $\|\Delta\|_\infty < 1$. The block diagram of the uncertain plant model for the piezo-actuated micropositioning system is shown in Fig. 5. According to this figure, the measured output voltage (v_y) can be computed as:

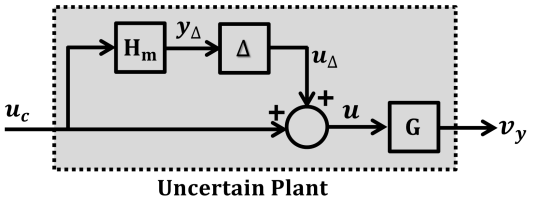

FIGURE 5. Uncertain plant with multiplicative input uncertainty.

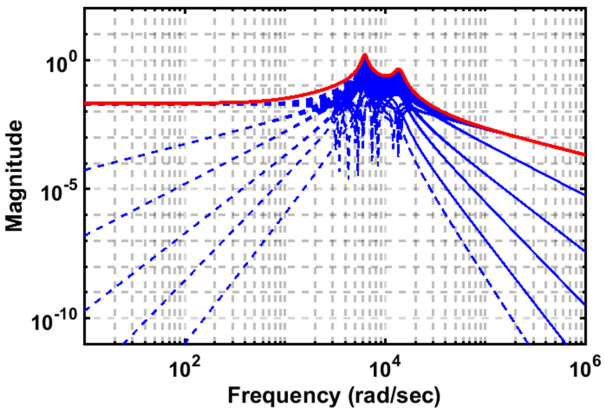

FIGURE 6. Relative error functions (dotted lines) with multiplicative uncertainty weighting function (solid line).

$$v_y = G_\Delta(s)u_c = G_\Delta(u_f + u_b) \tag{6}$$

where, u_f is the control action by the Dahl feedforward compensator and u_b is the control action by the feedback controller. In case of the considered multiplicative uncertainty, the relative error function E_m can be computed as:

$$E_m(\omega) = \max_{G_\Delta \in \Pi} \left| \frac{G_\Delta(j\omega) - G(j\omega)}{G(j\omega)} \right| \tag{7}$$

The identified parameters of the characteristic equation are considered to have three possible values: a nominal value and two possible values with $\pm 5\%$ variations around the nominal value. The total of 729 possible combinations of the relative error function are presented in Fig. 6 (dotted lines). The multiplicative uncertainty weighting function (H_m) is the bound on the multiplicative uncertainty and must be chosen in such a way that it satisfies the condition $|H_m(j\omega)| \geq E_m(\omega), \forall\omega$. In order to satisfy this condition, the multiplicative uncertainty weighting function (H_m) of 5^{th} order is designed as follows:

$$H_m(s) = \frac{g(s^2 + 2\zeta_1\omega_1 s + \omega_1^2)(s^2 + 2\zeta_3\omega_2 s + \omega_2^2)(\epsilon s + \omega_3)}{(s^2 + 2\zeta_2\omega_1 s + \omega_1^2)(s^2 + 2\zeta_4\omega_2 s + \omega_2^2)(s + \omega_3/M)} \tag{8}$$

This transfer function is achieved by connecting two normalized inverse notch filters' transfer functions with a low pass filter transfer function in series. The parameter values of the uncertainty weighting function are presented in *Table 2*. The achieved multiplicative uncertainty weighting function is presented in Fig. 6 (solid line). It is clear from this Fig. 6

TABLE 2. Parameter values of multiplicative uncertainty weighting function.

Parameter:	g	ζ_1	ζ_2	ζ_3	ζ_4
Value:	0.02	3.5	0.05	0.7	0.08
Parameter:	ω_1	ω_2	ω_3	M	ϵ
Value:	6.3×10^3	1.4×10^4	1×10^4	1	1×10^{-8}

that the proposed uncertainty weighting function satisfies the desired condition of $|H_m(j\omega)| \geq E_m(\omega), \forall\omega$.

C. DAHL HYSTERESIS MODEL

As mentioned earlier in *Section I* that there are several hysteresis models which have been investigated in the literature. Some of the most commonly used hysteresis models are operator based models and some are differential based models. A common practice, to compensate hysteresis nonlinearity, is first to find out the inverse of these hysteresis models and then to cascade the inverse model, as a feedforward compensator, with the actuator. Calculating the inverse hysteresis model is often a challenging task due to its computational complexity. Other than computational complexity of inverse model calculation, real-time implementation, accuracy as well as identification process of finding parameters of the hysteresis model are other factors which must be considered for selecting a proper hysteresis model.

In this article, the differential based model, particularly the Dahl hysteresis model, is considered as calculating the inverse hysteresis model, as a feedforward compensator, for an operator based model involves computational inverse modeling complexity. Dahl hysteresis model is based on the differential equation like Bouc-Wen or Duhem hysteresis models. The reason for opting Dahl hysteresis model for the considered piezoelectric actuator is its simplicity in implementation and also good accuracy in representing a large class of hysteresis. According to [12], the Dahl hysteresis model can have better accuracy than the Bouc-Wen hysteresis model with the same number of unknown model parameters. As far as Duhem hysteresis model is concerned, obtaining an inverse hysteresis model as well as the identification process of Duhem hysteresis model is not easy. All necessary details about the considered Dahl hysteresis model can be found in [44].

The Dahl hysteresis model for the piezoelectric actuator can be represented with a second-order state-space model. The state equations are:

$$\dot{z}(t) = A_H z(t)\dot{x}_a(t) + B_H \dot{x}_a(t) \tag{9}$$

$$\begin{bmatrix}\dot{z}_1(t)\\ \dot{z}_2(t)\end{bmatrix} = \underbrace{\begin{bmatrix}0 & 1\\ -\alpha_2 & -\alpha_1 sgn\,(\dot{x}_a(t))\end{bmatrix}}_{A_H}\begin{bmatrix}z_1(t)\\ z_2(t)\end{bmatrix}\dot{x}_a(t) + \underbrace{\begin{bmatrix}0\\ \gamma_a\end{bmatrix}}_{B_H}\dot{x}_a(t) \tag{10}$$

where, $z_1(t)$ and $z_2(t)$ are two intermediate state variables, $x_a(t)$ displacement of the piezoelectric actuator and α_1, α_2 and γ_a are constant parameters. The nonlinear hysteretic effect $H(t)$ of the actuator can be represented by the following output equation:

$$H(t) = C_H z(t) \tag{11}$$

$$H(t) = \underbrace{\begin{bmatrix}\beta_2 & \beta_1 sgn\,(\dot{x}_a(t))\end{bmatrix}}_{C_H}\begin{bmatrix}z_1(t)\\ z_2(t)\end{bmatrix} \tag{12}$$

where, β_1 and β_2 are constant parameters. All constant parameters of the Dahl hysteresis model govern the shape and amplitude of the hysteresis loop. The solution of the Dahl state-space model will be used to determine the actual displacement of the piezoelectric actuator, which can be described as:

$$x_a(t) = g_a v_a(t) - H(t) \tag{13}$$

where, g_a is a piezoelectric coefficient and $v_a(t)$ is the applied input voltage to the piezoelectric actuator.

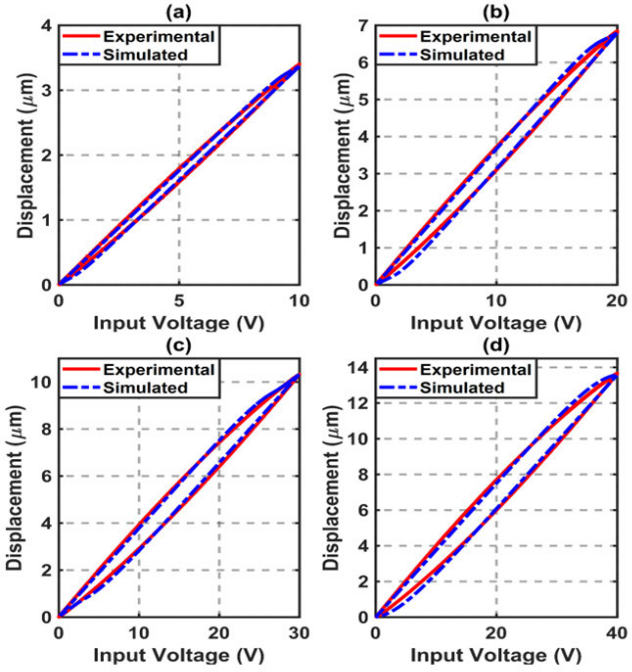

FIGURE 7. Experimental and simulated (with Dahl hysteresis model) hysteresis loops with input voltage of (a) 10V (b) 20V (c) 30V (d) 40V to piezoelectric actuator.

All parameters of the Dahl hysteresis model with piezoelectric coefficient are identified from the real-time experimental data. For this purpose, triangular input voltages of different amplitudes, in order to achieve multiple positioning ranges, and frequency of 10 Hz are applied to the piezoelectric actuator. In order to identify the parameters of the Dahl hysteresis model, a nonlinear curve-fitting problem is solved in a least-square sense by using the nonlinear optimization toolbox in the MATLAB. The identified parameters of Dahl hysteresis model with piezoelectric coefficient are: $\alpha_1 = 1.76\times10^3, \alpha_2 = 3.46\times10^7, \beta_1 = 0, \beta_2 = 3.11\times10^7$, $\gamma_a = 30$ and $g_a = 0.925$. The experimental and simulated hysteresis loops are presented in Fig. 7(a) to Fig. 7(d).

In all these figures, a close match between the experimental and simulated hysteresis loops validates the Dahl hysteresis model for the considered piezoelectric actuator.

IV. CONTROL DESIGN FOR PIEZO-ACTUATED MICROPOSITIONING STAGE

In this section, first of all, the Dahl feedforward compensator is designed to deal with hysteresis nonlinearity of the piezoelectric actuator. Next, μ-synthesis robust feedback controller is designed, for uncertain system model, to achieve precise reference tracking. After the controller design, nominal as well as robust stability and robust performance of the closed-loop system is analyzed.

A. DAHL FEEDFORWARD COMPENSATOR DESIGN

A common practice to compensate the effects of nonlinear hysteresis phenomenon is to design an inverse hysteresis model and then to use it as a feedforward compensator. Calculation of inverse hysteresis model is often cumbersome which introduces inverse modeling complexity. To avoid this complexity, a new simple approach of hysteresis compensation is presented here. According to this approach, there is no need to perform inversion of the hysteresis model, rather than only inverse of the piezoelectric coefficient (which is strictly positive) is required. The output voltage ($u_f(t)$) of Dahl hysteresis feedforward compensator can be computed as:

$$u_f(t) = \frac{1}{g_a}\left(x_r(t) + H(t)\right) \tag{14}$$

where, $x_r(t)$ is the desired displacement of the piezoelectric actuator. The desired displacement of the piezoelectric actuator is related to the reference input voltage ($v_r(t)$) through a gain of 3 μm/V. For example, in order to achieve the desired displacement of 12 μm, the reference input voltage of 4 V must be applied. This output voltage ($u_f(t)$) of Dahl hysteresis feedforward compensator will be added with the output voltage ($u_b(t)$) of the robust feedback controller to generate the control input ($u_c(t)$) for the micropositioning system.

The simulation results of hysteresis compensation with Dahl feedforward compensator is presented in Fig. 8. This achieved result indicates the perfect compensation of nonlinear hysteresis phenomenon with the presented feedforward compensator approach. Slight hysteresis nonlinearity still can be observed in the real-time experimental results due to some mismatch between the experimental and simulated hysteresis loops.

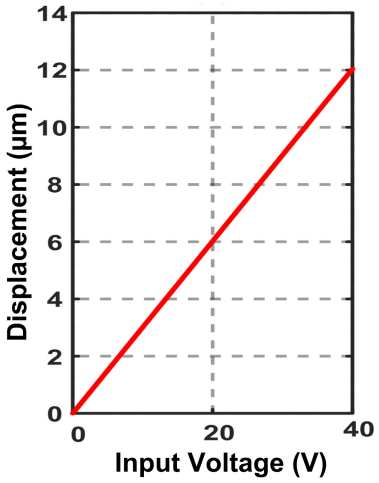

FIGURE 8. Simulation result of hysteresis compensation with Dahl feedforward compensator.

B. μ-SYNTHESIS ROBUST FEEDBACK CONTROLLER DESIGN

To enhance the tracking performance of the considered piezo-actuated micropositioning stage, a μ-synthesis robust feedback controller is designed for LTI dynamic model in the presence of model uncertainties. As hysteresis nonlinearity is well compensated by the proposed Dahl feedforward compensator, hysteresis nonlinearity as well as its compensator is not considered in the design of the feedback controller.

Desired Tracking Performance: The objective of the presented control scheme is to achieve not only nominal stability and nominal performance, but also the robust stability and the robust performance. The desired performance of the considered piezo-actuated micropositioning stage is to achieve precise reference tracking of 12 μm. As the tracking error increases with the increase of the tracking frequency, the peak-to-peak tracking error must be less than 1% for the tracking frequency till 10 Hz and less than 5% for the maximum tracking frequency of 50 Hz.

The general control configuration, used for μ-synthesis robust feedback controller design, is presented in Fig. 9. In order to achieve the desired performance specifications, two performance weighting functions (H_e and H_y) have been imposed in the control loop: H_e over the error voltage (v_e) and H_y over the output measured voltage (v_y), as shown in Fig. 9, where y_1 and y_2 are two controlled outputs. The performance weighting function (H_e) is designed by considering the desired performance in terms of small tracking error, large bandwidth and good robustness w.r.t. model uncertainties. H_y is designed in order to achieve good reference tracking, better noise rejection and to limit the overshoots. The designed performance weighting functions are:

$$H_e(s) = \frac{\frac{s}{M_e} + \omega_e}{s + \omega_e\epsilon_e}, \quad H_y(s) = \left(\frac{s + \frac{\omega_y}{M_y}}{\epsilon_y s + \omega_y}\right)^2 \tag{15}$$

where, $M_e = 2$, $\epsilon_e = 0.003$, $\omega_e = 1.26 \times 10^3$ rad/sec, $M_y = 1.5$, $\epsilon_y = 0.0001$ and $\omega_y = 7.5 \times 10^3$ rad/sec.

As shown in Fig. 9, $P(s)$ represents the generalized plant model, having a nominal plant model (G) with the uncertainty weighting function (H_m) as well as with two performance weighting functions (H_e and H_y). $K(s)$ represents the dynamics of the feedback controller. The generalized plant model, $P(s)$, having input vector $[u_\Delta \quad v_r \quad u_b]^T$ and output vector

TABLE 3. Conditions for closed-loop nominal and robust stability and performance.

Items	Conditions	Explanation
Nominal Stability	Matrix M is internally stable.	All four closed-loop sensitivity functions (**S**, **T**, **KS** and **GS**) must be stable.
Nominal Performance	$\|M_{22}\|_\infty < 1$	As $M_{22} = \begin{bmatrix} H_e\mathbf{S} \\ H_y\mathbf{T} \end{bmatrix}$ that's why $\|H_e\mathbf{S}\|_\infty < 1$, $\|H_y\mathbf{T}\|_\infty < 1$. $\Rightarrow \|\mathbf{S}(j\omega)\| < 1/\|H_e(j\omega)\|, \forall\omega$ and $\|\mathbf{T}(j\omega)\| < 1/\|H_y(j\omega)\|, \forall\omega$
Robust Stability	$\mu_{\Delta_r}(M_{11}(j\omega)) < 1, \forall\omega$	Here $M_{11} = -H_m\mathbf{T}$ and μ represents the structured singular value.
Robust Performance	$\mu_{\Delta}(M(j\omega)) < 1, \forall\omega$	Here $M = \begin{bmatrix} -H_m\mathbf{T} & H_m\mathbf{KS} \\ -H_e\mathbf{GS} & H_e\mathbf{S} \\ H_y\mathbf{GS} & H_y\mathbf{T} \end{bmatrix}$

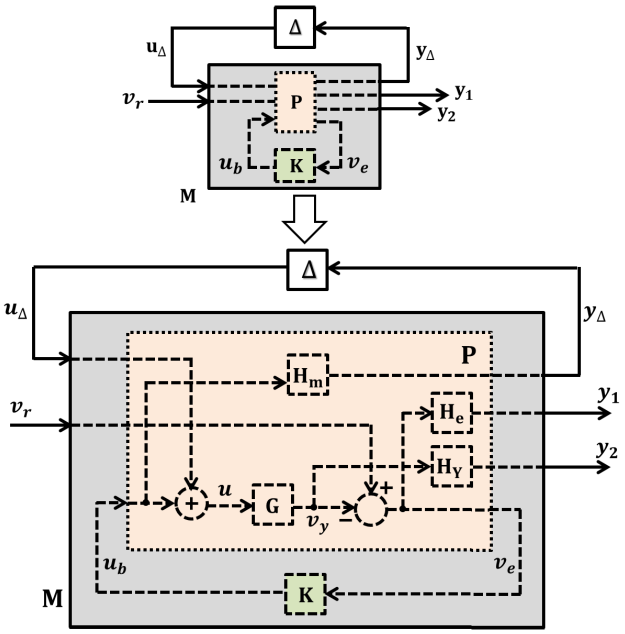

FIGURE 9. General control configuration for μ-synthesis robust feedback.

$[y_\Delta \;\; y_1 \;\; y_2 \;\; v_e]^T$, as shown in Fig. 9, can be described as:

$$\begin{bmatrix} y_\Delta \\ y_1 \\ y_2 \\ v_e \end{bmatrix} = \underbrace{\begin{bmatrix} 0 & 0 & H_m \\ -H_eG & H_e & -H_eG \\ H_yG & 0 & H_yG \\ -G & 1 & -G \end{bmatrix}}_{P(s)} \begin{bmatrix} u_\Delta \\ v_r \\ u_b \end{bmatrix} \tag{16}$$

If $P(s) = \begin{bmatrix} P_{11}(s) & P_{12}(s) \\ P_{21}(s) & P_{22}(s) \end{bmatrix}$ then $P_{11} = \begin{bmatrix} 0 & 0 \\ -H_eG & H_e \\ H_yG & 0 \end{bmatrix}$, $P_{12} = \begin{bmatrix} H_m \\ -H_eG \\ H_yG \end{bmatrix}$, $P_{21} = \begin{bmatrix} -G & 1 \end{bmatrix}$ and $P_{22} = -G$. The generalized plant model $P(s)$ can be combined with the designed controller transfer function $K(s)$ via the lower linear fractional transformation (LFT) to yield the transfer function matrix $M(s)$ as:

$$M = F_l(P, K) = P_{11} + P_{12}K(1 - P_{22}K)^{-1}P_{21} \tag{17}$$

Matrix $M(s)$, having input vector $[u_\Delta \;\; v_r]^T$ and output vector $[y_\Delta \;\; y_1 \;\; y_2]^T$ can be described as:

$$\begin{bmatrix} y_\Delta \\ y_1 \\ y_2 \end{bmatrix} = \underbrace{\begin{bmatrix} -H_m\mathbf{T} & H_m\mathbf{KS} \\ -H_e\mathbf{GS} & H_e\mathbf{S} \\ H_y\mathbf{GS} & H_y\mathbf{T} \end{bmatrix}}_{M(s)} \begin{bmatrix} u_\Delta \\ v_r \end{bmatrix} \tag{18}$$

If $M(s) = \begin{bmatrix} M_{11}(s) & M_{12}(s) \\ M_{21}(s) & M_{22}(s) \end{bmatrix}$ then $M_{11} = -H_m\mathbf{T}$, $M_{12} = H_m\mathbf{KS}$, $M_{21} = \begin{bmatrix} -H_e\mathbf{GS} \\ H_y\mathbf{GS} \end{bmatrix}$ and $M_{22} = \begin{bmatrix} H_e\mathbf{S} \\ H_y\mathbf{T} \end{bmatrix}$. Here, **S**, **T**, **KS** and **GS** represent four closed-loop sensitivity functions which are classically defined as:

$$\mathbf{S} = \frac{1}{1 + K(s)G(s)}, \quad \mathbf{T} = \frac{K(s)G(s)}{1 + K(s)G(s)}, \tag{19}$$

$$\mathbf{KS} = \frac{K(s)}{1 + K(s)G(s)}, \quad \mathbf{GS} = \frac{G(s)}{1 + K(s)G(s)} \tag{20}$$

Now, in order to analyze the robust stability and robust performance of the closed-loop system, the structure of Δ matrix is defined as:

$$\Delta = \left\{ \begin{bmatrix} \Delta_f & 0 \\ 0 & \Delta_r \end{bmatrix}, \Delta_f \in C^{2\times1}, \Delta_r \in C^{1\times1} \right\} \subset C^{3\times2} \tag{21}$$

Here, the first block Δ_f of structured uncertainty represents the fictitious block with inputs $[y_1 \;\; y_2]^T$ and output v_r. The second block Δ_r of structured uncertainty represents the real parametric uncertainties with input y_Δ and output u_Δ. The necessary conditions for nominal as well as robust stability and performance are presented in *Table 3*.

The design of performance weighting functions (H_e and H_y) is an important step for the design of the considered μ-synthesis robust feedback controller. The formula (15) for H_e has been proposed by keeping in mind that the inverse of this performance weighting function imposes the upper bound (template) over the closed-loop output sensitivity function **S** (as mentioned for the nominal performance condition in Table 3). Ideally, **S** must provide maximum attenuation in the low frequency area in order to minimize the tracking error, large bandwidth (corresponds to a faster rise time) and $\|\mathbf{S}\|_\infty$ less than 6 dB in order to achieve good robustness w.r.t. model uncertainties.

The performance weighting function H_e has three variables (ϵ_e, M_e and ω_e) in (15) and the values of these variables help to adjust the template in order to achieve the best possible shape of the closed-loop output sensitivity function **S**. The value of ϵ_e moves the template upward or downward in low frequency, M_e moves the template upward or downward in high frequency and ω_e moves the template left or right to achieve the best possible bandwidth. Similarly, the inverse of performance weighting function H_y imposes the upper bound (template) over the closed-loop complementary sensitivity function **T** (as mentioned for the nominal performance condition in Table 3). Ideally, **T** must remain at 0 dB in low frequencies in order to achieve unity feedback gain, must provide maximum attenuation in high frequencies for better noise rejection and $\|\mathbf{T}\|_\infty$ less than 3.5 dB in order to limit the overshoots. The values of three variables (ϵ_y, M_y and ω_y) of the performance weighting function H_y in (15) help to adjust the template over **T** in order to achieve its desired shape. DK-iteration method is used in order to design the μ-synthesis robust feedback controller. The starting point of this iterative method is the upper bound on μ in terms of the scaled maximum singular value ($\bar{\sigma}$) as:

$$\mu_\Delta(M) \leq \min_{D\in D_\Delta} \bar{\sigma}\left(DMD^{-1}\right) \tag{22}$$

where, D_Δ is the set of matrices with the property that $D\Delta = \Delta D$ for every $D \in D_\Delta$. Now, the idea of μ-synthesis robust feedback controller is to minimize, over all stabilizing controllers $K(s)$, the peak value over frequency of this upper bound of μ:

$$\min_K \left(\min_{D\in D_\Delta} \|DF_l(P,K)D^{-1}\|_\infty\right) \tag{23}$$

Further necessary details about DK-iteration procedure can be found in [45]. The achieved controller transfer function is of 36^{th} order with upper bound of μ is 0.71. For the real-time implementation, the order of the controller transfer function is reduced. For this purpose, first the Hankel singular values are computed and then the states with relatively small Hankel singular values are discarded. Finally, the achieved 6^{th} order controller transfer function is given as follows:

$$K(s) = \frac{n_5 s^5 + n_4 s^4 + n_3 s^3 + n_2 s^2 + n_1 s + n_0}{s^6 + d_5 s^5 + d_4 s^4 + d_3 s^3 + d_2 s^2 + d_1 s + d_0} \tag{24}$$

where, $n_0 = 4.73\times10^{22}$, $n_1 = 1.51\times10^{22}$, $n_2 = 7.66\times10^{17}$, $n_3 = 1.04\times10^{15}$, $n_4 = 1.78\times10^{10}$, $n_5 = 5.29\times10^{6}$, $d_0 = 7.79\times10^{19}$, $d_1 = 4.71\times10^{19}$, $d_2 = 7.38\times10^{18}$, $d_3 = 7.86\times10^{14}$, $d_3 = 3.21\times10^{10}$ and $d_3 = 4.69\times10^{5}$. The stability and performance analysis of the closed-loop system is presented in the next sub-section.

C. CLOSED-LOOP STABILITY AND PERFORMANCE ANALYSIS

1) CLOSED-LOOP NOMINAL STABILITY

In order to analyze the closed-loop nominal stability, the step responses of all four closed-loop sensitivity functions (**S**, **T**, **KS** and **GS**) are presented in Fig. 10. This figure demonstrates that all four closed-loop sensitivity functions are stable, which is the necessary condition for having the closed-loop nominal stability as mentioned in Table 3. The step response (Fig. 10(a)) of the output sensitivity function (**S**) shows the behavior of the error voltage (v_e) w.r.t. reference voltage (v_r). It is evident from this step response that $v_e \to 0$ as time $t \to \infty$. The step response (Fig. 10(b)) of the complementary sensitivity function (**T**) shows the behavior of the output voltage (v_y) w.r.t. reference input voltage (v_r). It is evident from this step response that the closed-loop system has unity feedback gain with good transient characteristics. The step response (Fig. 10(c)) of the input sensitivity function (**KS**) shows the behavior of the control input (u_c) w.r.t. reference voltage (v_r). The step response (Fig. 10(d)) of plant sensitivity function (**GS**) shows the behavior of the output voltage (v_y) w.r.t. any possible disturbance at the system input. It shows that any input disturbance will be well rejected by the presented control scheme.

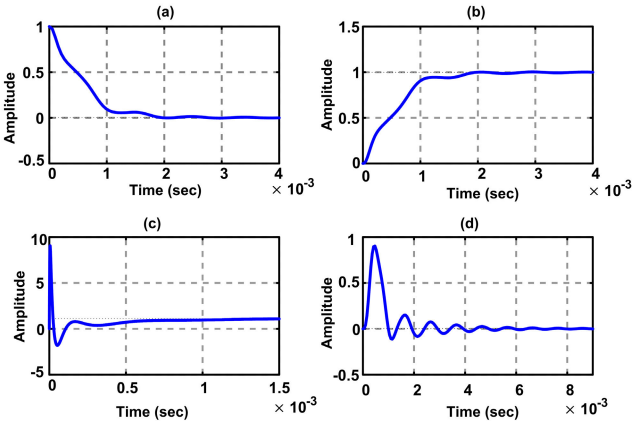

FIGURE 10. Step response of (a) output sensitivity function S (b) complementary sensitivity function T (c) input sensitivity function KS (d) plant sensitivity function GS to demonstrate the nominal stability of the closed-loop system.

2) CLOSED-LOOP NOMINAL PERFORMANCE

In order to analyze the nominal performance of the closed-loop system, the conditions mentioned in *Table 3* must be verified. The desired conditions of nominal performance are well achieved as $\|H_e\mathbf{S}\|_\infty = 0.81$ and $\|H_y\mathbf{T}\|_\infty = 0.92$. As the achieved $\|H_e\mathbf{S}\|_\infty < 1$ and $\|H_y\mathbf{T}\|_\infty < 1$, it means $|\mathbf{S}(j\omega)| < 1/|H_e(j\omega)|, \forall\omega$ and $|\mathbf{T}(j\omega)| < 1/|H_y(j\omega)|, \forall\omega$ which is also evident from the Fig. 11(a) and Fig. 11(b), respectively. This figure shows that the two sensitivity functions **S** and **T** remain under the templates which were imposed by the inverse of the performance weighting functions H_e and H_y respectively.

3) CLOSED-LOOP ROBUST STABILITY

In order to analyze the robust stability of the closed-loop system with model uncertainty, the μ plot, as per the condition mentioned in *Table 3*, is presented in Fig. 12(a). According to

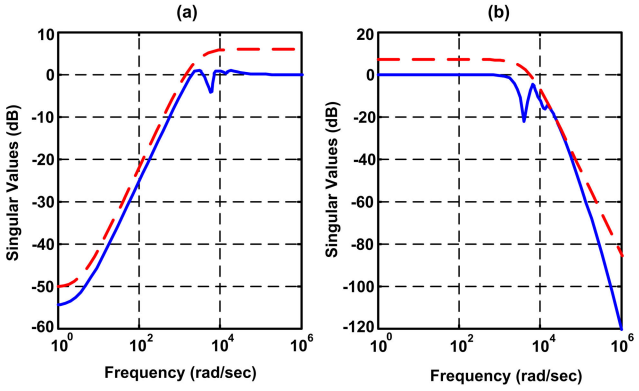

FIGURE 11. (a) Output sensitivity function (S) (solid line) (b) complimentary sensitivity function (T) (solid line) with inverse of their corresponding performance weighting functions (dotted lines) to demonstrate closed-loop nominal performance.

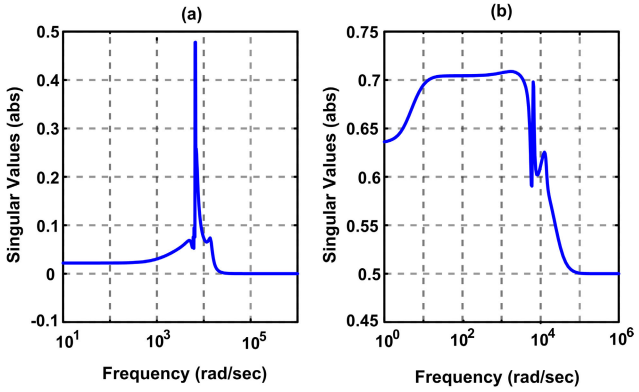

FIGURE 12. Structured singular values (μ) to demonstrate (a) closed-loop robust stability and (b) closed-loop robust performance.

this figure, the desired condition of robust stability is satisfied with the maximal value of μ is 0.48 which must be less than unity. It means that the closed-loop stability is guaranteed for all perturbations Δ with $\|\Delta\|_\infty < 1/0.48 = 2.08$.

4) CLOSED-LOOP ROBUST PERFORMANCE

Robust performance of the closed-loop system is also achieved as the desired condition, mentioned in *Table 3*, is satisfied and presented in Fig. 12(b). In this case, the achieved maximal value of μ is 0.71. It means that the robust performance of the closed-loop system is ensured for all perturbations Δ with $\|\Delta\|_\infty < 1/0.71 = 1.41$.

V. EXPERIMENTAL RESULTS

In this section, real-time experimental results are presented for the validation of the presented control scheme. All experiments are performed with the sampling frequency of 10 kHz. The triangular reference trajectories are selected in this article for an extensive real-time experimental analysis to verify the performance of the presented control scheme. Unlike sinusoidal trajectories, which are smooth trajectories, the triangular trajectories are non-smooth trajectories and contain high frequency harmonic components, increasing the difficulty in control. The triangular trajectories are widely utilized in many applications and a very common application is the scanning probe microscopy where a sample surface is scanned to generate its topographic image with an atomic-scale resolution.

A. HYSTERESIS COMPENSATION

In this sub-section, the inherent nonlinear hysteresis phenomenon of the piezoelectric actuator is analyzed in open-loop (without any compensator and with Dahl feedforward compensator) as well as in closed-loop with the presented control scheme (μ-synthesis robust feedback controller combined with the Dahl feedforward compensator). This analysis is performed with the real-time experimental results by applying multiple triangular input voltages of 10 V, 20 V, 30 V and 40 V to the piezoelectric actuator with tracking frequency of 10 Hz. The reason for selecting multiple input voltages is to demonstrate the effectiveness of the presented control scheme in compensating the hysteresis nonlinearity.

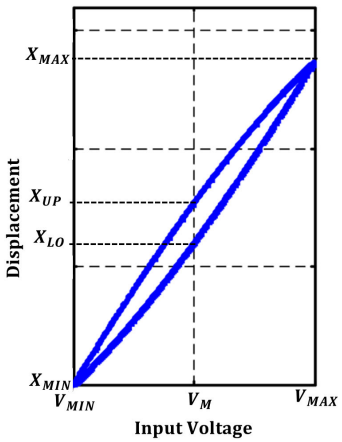

FIGURE 13. Hysteresis percentage calculation.

Hysteresis percentage is calculated in order to analyze the performance w.r.t. hysteresis compensation. To calculate the hysteresis percentage, first, the midpoint of the applied input voltage (V_M) to the piezoelectric actuator is calculated by using the following midpoint formula as shown in Fig. 13:

$$V_M = \left(\frac{V_{MAX} - V_{MIN}}{2}\right) + V_{MIN} \tag{25}$$

where, V_{MAX} and V_{MIN} are the applied maximum and minimum voltages to the piezoelectric actuator respectively. The displacements (X_{UP} and X_{LO}) of the piezoelectric actuator, as shown in Fig. 13, corresponding to the midpoint of the applied input voltage (V_M) is noted which is used to calculate the hysteresis percentage as:

$$Hysteresis\ \% = \left|\frac{X_{UP} - X_{LO}}{X_{MAX} - X_{MIN}}\right| \times 100 \tag{26}$$

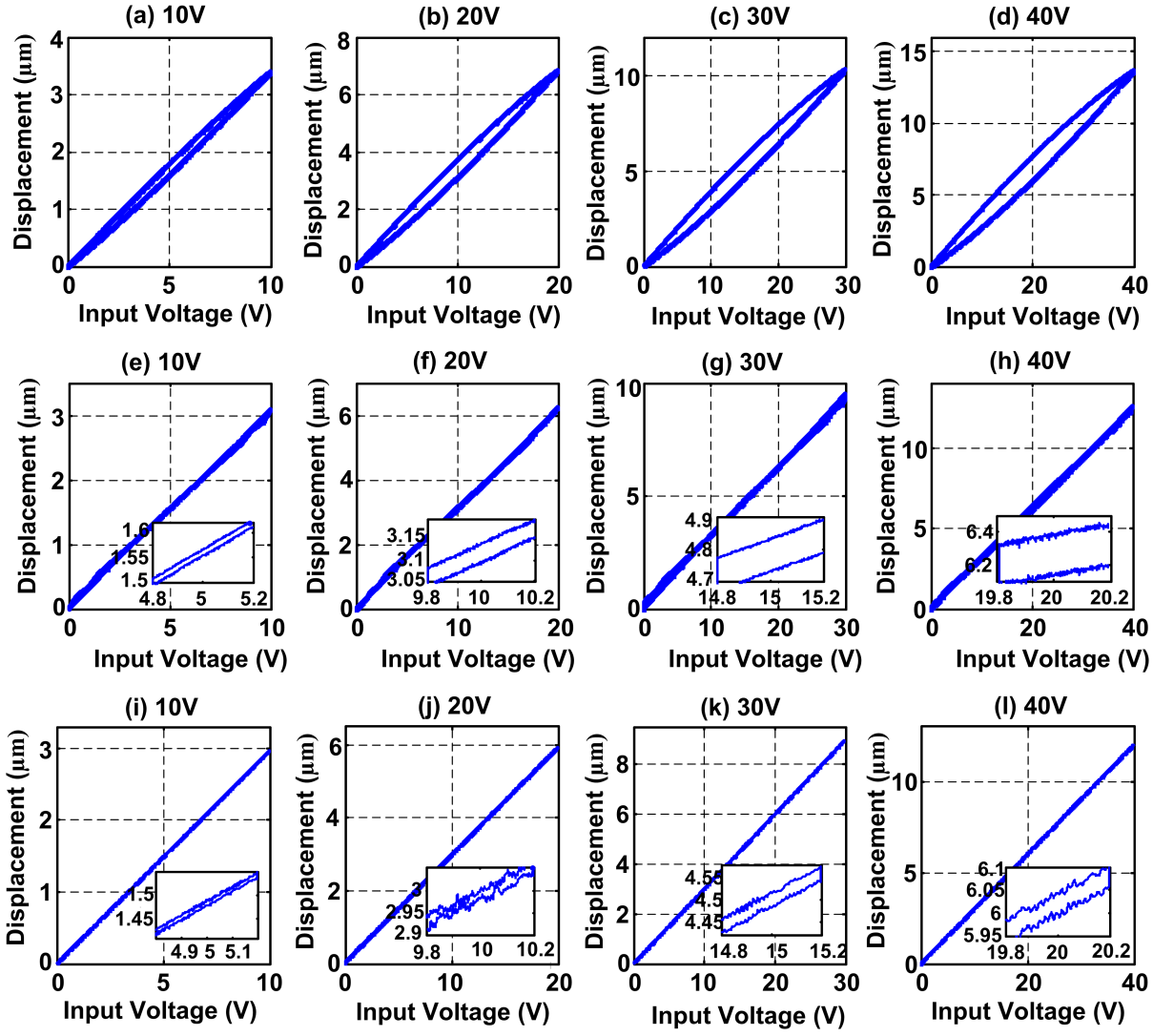

FIGURE 14. Experimental results of hysteresis loops at different input voltages of 10V, 20V, 30V and 40V to piezoelectric actuator with tracking frequency of 10 Hz (a)-(d) open loop configuration with no compensator (e)-(h) open-loop configuration with Dahl feedforward compensator (i)-(l) closed-loop configuration with a control scheme having μ-synthesis robust feedback controller with Dahl feedforward compensator.

where, X_{MAX} and X_{MIN} are the displacements of the piezoelectric actuator corresponding to applied input voltages of V_{MAX} and V_{MIN} respectively.

Hysteresis percentages of 6.19%, 9.08%, 11.16% and 12.44% are observed in the open-loop configuration without any compensator, as shown in Fig. 14(a) to Fig. 14(d), whereas 0.45%, 0.81%, 1.23% and 2.12% are achieved with Dahl feedforward compensator, as presented in Fig. 14(e) to Fig. 14(h), corresponding to input voltages of 10 V, 20 V, 30 V and 40 V respectively to the piezoelectric actuator. These results demonstrate the effectiveness of the Dahl feedforward compensator as an improvement of 92.73%, 91.07%, 88.98% and 82.96% is achieved in compensating the hysteresis nonlinearity as compared to the open-loop case without any compensator, corresponding to input voltages from 10 V to 40 V respectively. To further compensate the hysteresis nonlinearity, analysis is finally performed in closed-loop with the presented closed-loop control scheme. In this case, hysteresis percentages of 0.31%, 0.37%, 0.41% and 0.44% are observed corresponding to the input voltages of 10 V, 20 V, 30 V and 40 V respectively, as shown in Fig. 14(i) to Fig. 14(l). In this case, the improvements of 94.99%, 95.93%, 96.33% and 96.46% as compared to the open-loop case without any compensator and 31.11%, 54.32%, 66.67% and 79.25% as compared to the Dahl feedforward compensator are achieved corresponding to the input applied voltages from 10 V to 40 V respectively. These achieved results demonstrate that the presented control scheme, which is the combination of the μ-synthesis robust feedback controller with Dahl feedforward compensator, can compensate the hysteresis nonlinearity of

TABLE 4. Hysteresis % with different input voltages to piezoelectric actuator for tracking frequency of 10*Hz*.

Hysteresis %	10 V	20 V	30 V	40 V
Case I: Open-loop without compensator	6.19	9.08	11.16	12.44
Case II: Open-loop with Dahl feedforward compensator	0.45	0.81	1.23	2.12
Case III: Closed-loop with proposed control scheme	0.31	0.37	0.41	0.44
Improvement (%) in CASE II w.r.t. CASE I	92.73	91.07	88.98	82.96
Improvement (%) in CASE III w.r.t. CASE I	94.99	95.93	96.33	96.46
Improvement (%) in CASE III w.r.t. CASE II	31.11	54.32	66.67	79.25

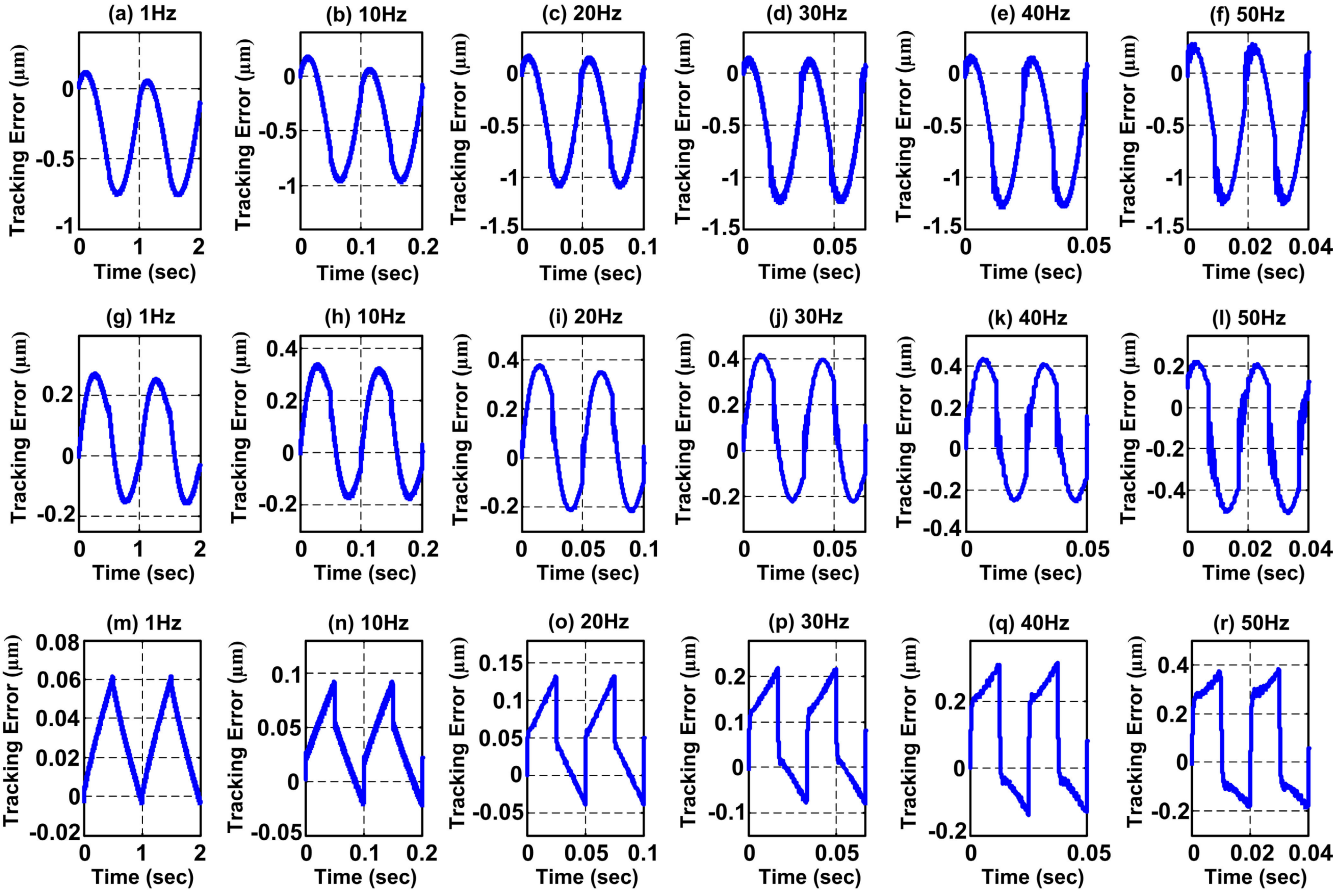

FIGURE 15. Experimental results of tracking error with triangular trajectories from 1 Hz to 50 Hz for the desired displacement of 12μm with (a)-(f) open-loop configuration without any compensator (g)-(l) open-loop configuration with Dahl feedforward compensator (m)-(r) closed-loop configuration with a control scheme having μ-synthesis robust feedback controller with Dahl feedforward compensator.

the piezoelectric actuator better than the Dahl feedforward compensator only. The summary of the achieved results is presented in *Table 4*.

B. TRACKING ERROR ANALYSIS

In this sub-section, the real-time tracking error between the desired triangular displacement of 12 μm with multiple tracking frequencies of 1 Hz, 10 Hz, 20 Hz, 30 Hz, 40 Hz and 50 Hz and the actual displacement of the piezo-actuated micropositioning stage is analyzed. The experiments were performed with tracking frequency from 1 Hz to 50 Hz in order to demonstrate the capability of the suggested control scheme that it works effectively with motion trajectories of multiple frequencies. The parameters of the performance weighting functions (H_e and H_y) are chosen in such a way that the tracking error of less than 5% is achieved with the maximum considered tracking frequency of 50 Hz. Indeed, it is possible to work in a higher frequency but then the

TABLE 5. Tracking error with different tracking frequencies for the desired triangular displacement of 12μm.

Tracking Error %	1Hz	10Hz	20Hz	30Hz	40Hz	50Hz
Case I: Open-loop without compensator	7.33	9.47	10.56	11.72	12.13	12.98
Case II: Open-loop with Dahl feedforward compensator	3.54	4.29	4.93	5.28	5.72	6.19
Case III: Closed-loop with proposed control scheme	0.51	0.94	1.46	2.39	3.71	4.58
Improvement (%) in CASE II w.r.t. CASE I	51.71	54.69	53.31	54.95	52.84	52.31
Improvement (%) in CASE III w.r.t. CASE I	93.04	90.07	86.17	79.61	69.41	64.71
Improvement (%) in CASE III w.r.t. CASE II	85.59	78.09	70.39	54.73	35.14	26.01

parameters of the performance weighting functions need to be modified first in order to achieve the desired performance specifications. Working in higher frequency may also introduce the phenomenon of high frequency vibrations which motivates to incorporate some damping controller [46], [47] in order to damp the first resonant mode of the system and accordingly to suppress the high frequency vibrations.

While working in open-loop without any compensator, the tracking errors of 7.33%, 9.47%, 10.56%, 11.72%, 12.13% and 12.98% are observed, as shown in Fig. 15(a) to Fig. 15(f), whereas, with the Dahl feedforward compensator, the errors reduce to 3.54%, 4.29%, 4.93%, 5.28%, 5.72% and 6.19% corresponding to the tracking frequencies of 1 Hz, 10 Hz, 20 Hz, 30 Hz, 40 Hz and 50 Hz respectively, as presented in Fig. 15(g) to Fig. 15(l). These results show the corresponding improvement of 51.71%, 54.69%, 52.31%, 54.95%, 52.84% and 52.31% in reducing the tracking error with the Dahl feedforward compensator, however, the desired tracking performance is still not achieved.

The proposed control scheme (the combination of μ-synthesis robust feedback controller with Dahl feedforward compensator) is now analyzed to further enhance the real-time tracking performance. Now, the tracking errors of 0.51%, 0.94%, 1.46%, 2.39%, 3.71% and 4.58% are achieved with corresponding tracking frequencies from 1 Hz to 50 Hz respectively, as shown in Fig. 15(m) to Fig. 15(r). These achieved results show significant improvement in reducing the tracking error with the presented control scheme. The improvements of 93.04%, 90.07%, 86.17%, 79.61%, 69.41% and 64.71%, as compared to the open-loop results with no compensator, and 85.59%, 78.09%, 70.39%, 54.73%, 35.14% and 26.01%, as compared to the Dahl feedforward compensator, with corresponding tracking frequencies from 1 Hz to 50 Hz, are achieved respectively. These experimental results show that the desired tracking performance is achieved with the presented control scheme. The summary of achieved experimental results in terms of tracking error and the improvements are presented in *Table 5*.

It has been observed from the achieved experimental results that the feedforward compensator can reduce hysteresis percentage significantly but the desired tracking performance can not be achieved with only a feedforward compensator, particularly in the presence of model uncertainties and external disturbances. A feedback controller is indeed required to further enhance the tracking performance. It has also been observed that the tracking errors increase gradually as the tracking frequency increases. High frequency vibrations may also appear in the output displacement with high tracking speeds. Therefor, the control strategy needs to be adjusted accordingly. The desired tracking performance of the considered piezo-actuated positioning stage has been well achieved with the presented control scheme.

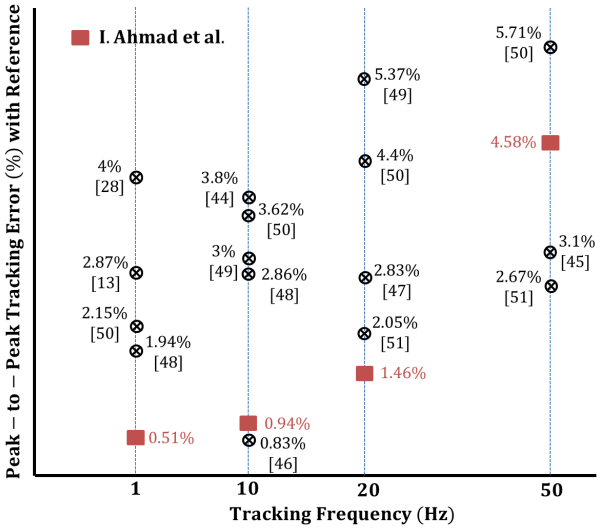

FIGURE 16. Performance comparison in terms of peak-to-peak tracking error with other papers in the literature.

The achieved real-time tracking performance in this article is now compared with some other combined feedforward-feedback control schemes presented in the literature [13], [28], [48]–[55]. A comparative study has been performed with those papers in the literature having real-time experimental results with similar tracking frequencies as presented in this article. Figure 16 shows the outcome of this comparison. Overall, it can be observed in Fig. 16 that the achieved peak-to-peak tracking error in this article is either

smaller than or comparable to the tracking errors presented in other papers.

VI. CONCLUSION

In this article, the real-time tracking performance of the piezo-actuated micropositioning stage has been analyzed in open-loop (without any compensator and with Dahl feedforward compensator) as well as in closed-loop with the proposed control scheme which combines the μ-synthesis robust feedback controller with the Dahl feedforward compensator. The plant model uncertainties are considered during the controller design in order to achieve the robust stability and the robust performance. Real-time experimental results demonstrate, for the input applied voltages from 10 V to 40 V to the piezoelectric actuator, an average improvement of 95.93% in terms of hysteresis compensation with the proposed feedback control scheme, as compared to the open-loop system without compensator, and 57.84% as compared to the Dahl feedforward compensator. Similarly, for the tracking frequency from 1 Hz to 50 Hz, an average improvement of 80.5%, in terms of tracking precision, is achieved with the proposed feedback control scheme, as compared to the open-loop system without compensator, and 58.33% as compared to the Dahl feedforward compensator. All the achieved experimental results demonstrate the effectiveness of the presented control scheme.

Further experimental analysis with circular or even random displacements as well as with some other advanced control algorithms will be performed in the prospective work. Control design for a 2D/3D micropositioning system, to deal with a major corresponding control issue of cross-coupling, will also be considered in the perspective work.

ACKNOWLEDGMENT

The authors extend their appreciation to the Deanship of Scientific Research at King Saud University for funding this work through research group no. RG-1439-028.

REFERENCES

[1] G.-Y. Gu, L.-M. Zhu, C.-Y. Su, H. Ding, and S. Fatikow, "Modeling and control of piezo-actuated nanopositioning stages: A survey," *IEEE Trans. Autom. Sci. Eng.*, vol. 13, no. 1, pp. 313–332, Jan. 2016.

[2] M. S. Rana, H. R. Pota, and I. R. Petersen, "A survey of methods used to control piezoelectric tube scanners in high-speed AFM imaging," *Asian J. Control*, vol. 20, no. 4, pp. 1379–1399, Jul. 2018.

[3] W. Zhang, M. Pang, and C. Ru, "Nanopositioning for lithography and data storage," in *Nanopositioning Technologies*. Cham, Switzerland: Springer, 2016, pp. 381–409.

[4] L. Zhang, K. Yao, E. Keikha, Y. F. Chen, M. A. Rahman, A. Al Mamun, and C. S. Bhatia, "Dual-stage nanopositioning scheme for 10 $Tbit/in^2$ hard disk drives with a shear-mode piezoelectric single-crystal microactuator," *IEEE Trans. Magn.*, vol. 51, no. 4, pp. 1–9, Apr. 2015.

[5] Z. Chen, D. Zhou, H. Liao, and X. Zhang, "Precision alignment of optical fibers based on telecentric stereo microvision," *IEEE/ASME Trans. Mechatronics*, vol. 21, no. 4, pp. 1924–1934, Aug. 2016.

[6] T. Dörfler, T. Eilert, C. Röcker, J. Nagy, and J. Michaelis, "Structural information from single-molecule FRET experiments using the fast nanopositioning system," *J. Vis. Exp.*, no. 120, Feb. 2017, Art. no. e54782.

[7] Z. Zhang, P. Yan, and G. Hao, "A large range flexure-based servo system supporting precision additive manufacturing," *Engineering*, vol. 3, no. 5, pp. 708–715, Oct. 2017.

[8] S. Devasia, E. Eleftheriou, and S. O. R. Moheimani, "A survey of control issues in nanopositioning," *IEEE Trans. Control Syst. Technol.*, vol. 15, no. 5, pp. 802–823, Sep. 2007.

[9] C. Ru, X. Liu, and Y. Sun, *Nanopositioning Technologies*. Cham, Switzerland: Springer, 2016.

[10] J. Gan, Z. Mei, X. Chen, Y. Zhou, and M. F. Ge, "A modified duhem model for rate-dependent hysteresis behaviors," *Micromachines*, vol. 10, no. 10, p. 680, Oct. 2019.

[11] D. Habineza, M. Rakotondrabe, and Y. Le Gorrec, "Bouc–Wen modeling and feedforward control of multivariable hysteresis in piezoelectric systems: Application to a 3-DoF piezotube scanner," *IEEE Trans. Control Syst. Technol.*, vol. 23, no. 5, pp. 1797–1806, Sep. 2015.

[12] Q. Xu and Y. Li, "Dahl model-based hysteresis compensation and precise positioning control of an XY parallel micromanipulator with piezoelectric actuation," *J. Dyn. Syst., Meas., Control*, vol. 132, no. 4, Jul. 2010, Art. no. 041011.

[13] M. Al Janaideh, M. Rakotondrabe, and O. Aljanaideh, "Further results on hysteresis compensation of smart micropositioning systems with the inverse Prandtl–Ishlinskii compensator," *IEEE Trans. Control Syst. Technol.*, vol. 24, no. 2, pp. 428–439, Mar. 2016.

[14] S. Xiao and Y. Li, "Modeling and high dynamic compensating the rate-dependent hysteresis of piezoelectric actuators via a novel modified inverse Preisach model," *IEEE Trans. Control Syst. Technol.*, vol. 21, no. 5, pp. 1549–1557, Sep. 2013.

[15] Y. Liu, D. Zou, H. Wu, and H. Liu, "Modelling and compensation of hysteresis in piezoelectric actuators based on Maxwell approach," *Electron. Lett.*, vol. 52, no. 3, pp. 188–190, Feb. 2016.

[16] Z. Li, J. Shan, and U. Gabbert, "Inverse compensation of hysteresis using Krasnoselskii–Pokrovskii model," *IEEE/ASME Trans. Mechatronics*, vol. 23, no. 2, pp. 966–971, Apr. 2018.

[17] M. Al Janaideh and O. Aljanaideh, "Further results on open-loop compensation of rate-dependent hysteresis in a magnetostrictive actuator with the Prandtl–Ishlinskii model," *Mech. Syst. Signal Process.*, vol. 104, pp. 835–850, May 2018.

[18] P.-B. Nguyen, S.-B. Choi, and B.-K. Song, "A new approach to hysteresis modelling for a piezoelectric actuator using Preisach model and recursive method with an application to open-loop position tracking control," *Sens. Actuators A, Phys.*, vol. 270, pp. 136–152, Feb. 2018.

[19] M. Ming, Z. Feng, J. Ling, and X.-H. Xiao, "Hysteresis modelling and feedforward compensation of piezoelectric nanopositioning stage with a modified Bouc–Wen model," *Micro Nano Lett.*, vol. 13, no. 8, pp. 1170–1174, Aug. 2018.

[20] M. Al Janaideh, M. Rakotondrabe, I. Al-Darabsah, and O. Aljanaideh, "Internal model-based feedback control design for inversion-free feedforward rate-dependent hysteresis compensation of piezoelectric cantilever actuator," *Control Eng. Pract.*, vol. 72, pp. 29–41, Mar. 2018.

[21] M. Rakotondrabe, "Bouc–Wen modeling and inverse multiplicative structure to compensate hysteresis nonlinearity in piezoelectric actuators," *IEEE Trans. Autom. Sci. Eng.*, vol. 8, no. 2, pp. 428–431, Apr. 2011.

[22] F. Wang, Z. Liu, Y. Zhang, and C. L. P. Chen, "Adaptive fuzzy control for a class of stochastic pure-feedback nonlinear systems with unknown hysteresis," *IEEE Trans. Fuzzy Syst.*, vol. 24, no. 1, pp. 140–152, Feb. 2016.

[23] X. Chen, C.-Y. Su, Z. Li, and F. Yang, "Design of implementable adaptive control for Micro/Nano positioning system driven by piezoelectric actuator," *IEEE Trans. Ind. Electron.*, vol. 63, no. 10, pp. 6471–6481, Oct. 2016.

[24] L. Cheng, W. Liu, Z.-G. Hou, J. Yu, and M. Tan, "Neural-network-based nonlinear model predictive control for piezoelectric actuators," *IEEE Trans. Ind. Electron.*, vol. 62, no. 12, pp. 7717–7727, Dec. 2015.

[25] Q. Xu, "Precision motion control of piezoelectric nanopositioning stage with chattering-free adaptive sliding mode control," *IEEE Trans. Autom. Sci. Eng.*, vol. 14, no. 1, pp. 238–248, Jan. 2017.

[26] M. Hammouche, P. Lutz, and M. Rakotondrabe, "Robust and optimal output-feedback control for interval state-space model: Application to a two-degrees-of-freedom piezoelectric tube actuator," *J. Dyn. Syst., Meas., Control*, vol. 141, no. 2, Feb. 2019, Art. no. 021008.

[27] I. Ahmad, "Two degree-of-freedom robust digital controller design with Bouc–Wen hysteresis compensator for piezoelectric positioning stage," *IEEE Access*, vol. 6, pp. 17275–17283, 2018.

[28] H. Tang and Y. Li, "Feedforward nonlinear PID control of a novel micromanipulator using Preisach hysteresis compensator," *Robot. Comput.-Integr. Manuf.*, vol. 34, pp. 124–132, Aug. 2015.

[29] S. A. Rios and A. J. Fleming, "Design of a charge drive for reducing hysteresis in a piezoelectric bimorph actuator," *IEEE/ASME Trans. Mechatronics*, vol. 21, no. 1, pp. 51–54, Feb. 2016.

[30] L. Liu, H. Yun, Q. Li, X. Ma, S.-L. Chen, and J. Shen, "Fractional order based modeling and identification of coupled creep and hysteresis effects in piezoelectric actuators," *IEEE/ASME Trans. Mechatronics*, vol. 25, no. 2, pp. 1036–1044, Apr. 2020.
[31] K. Kuhnen and P. Krejci, "Compensation of complex hysteresis and creep effects in piezoelectrically actuated systems—A new Preisach modeling approach," *IEEE Trans. Autom. Control*, vol. 54, no. 3, pp. 537–550, Mar. 2009.
[32] H. Janocha and K. Kuhnen, "Real-time compensation of hysteresis and creep in piezoelectric actuators," *Sens. Actuators A, Phys.*, vol. 79, no. 2, pp. 83–89, Feb. 2000.
[33] S. S. Aphale, S. Devasia, and S. O. Reza Moheimani, "High-bandwidth control of a piezoelectric nanopositioning stage in the presence of plant uncertainties," *Nanotechnology*, vol. 19, no. 12, Mar. 2008, Art. no. 125503.
[34] S. S. Aphale, S. Devasia, and S. O. R. Moheimani, "Achieving high-bandwidth nanopositioning in presence of plant uncertainties," in *Proc. IEEE/ASME Int. Conf. Adv. Intell. Mechatronics*, Jul. 2008, pp. 943–948.
[35] T. M. Duc, N. Van Hoa, and T.-P. Dao, "Adaptive fuzzy fractional-order nonsingular terminal sliding mode control for a class of second-order nonlinear systems," *J. Comput. Nonlinear Dyn.*, vol. 13, no. 3, Mar. 2018, Art. no. 031004.
[36] L. Ma, X. Huo, X. Zhao, and G. Zong, "Adaptive fuzzy tracking control for a class of uncertain switched nonlinear systems with multiple constraints: A small-gain approach," *Int. J. Fuzzy Syst.*, vol. 21, no. 8, pp. 2609–2624, Nov. 2019.
[37] Y. Chang, Y. Wang, F. E. Alsaadi, and G. Zong, "Adaptive fuzzy output-feedback tracking control for switched stochastic pure-feedback nonlinear systems," *Int. J. Adapt. Control*, vol. 33, no. 10, pp. 1567–1582, 2019.
[38] L. Ma, N. Xu, X. Huo, and X. Zhao, "Adaptive finite-time output-feedback control design for switched pure-feedback nonlinear systems with average dwell time," *Nonlinear Anal., Hybrid Syst.*, vol. 37, Aug. 2020, Art. no. 100908.
[39] X. H. Chang, J. H. Park, and J. Zhou, "Robust static output feedback H_∞ control design for linear systems with polytopic uncertainties," *Syst. Control Lett.*, vol. 85, pp. 23–32, Nov. 2015.
[40] T.-P. Dao and S.-C. Huang, "Design and analysis of a compliant micro-positioning platform with embedded strain gauges and viscoelastic damper," *Microsyst. Technol.*, vol. 23, no. 2, pp. 441–456, Feb. 2017.
[41] T.-P. Dao, N. L. Ho, T. T. Nguyen, H. G. Le, P. T. Thang, H.-T. Pham, H.-T. Do, M.-D. Tran, and T. T. Nguyen, "Analysis and optimization of a micro-displacement sensor for compliant microgripper," *Microsyst. Technol.*, vol. 23, no. 12, pp. 5375–5395, Dec. 2017.
[42] N. L. Ho, T.-P. Dao, H. G. Le, and N. L. Chau, "Optimal design of a compliant microgripper for assemble system of cell phone vibration motor using a hybrid approach of ANFIS and Jaya," *Arabian J. Sci. Eng.*, vol. 44, no. 2, pp. 1205–1220, Feb. 2019.
[43] L. Dugard and I. D. Landau, "Recursive output error identification algorithms theory and evaluation," *Automatica*, vol. 16, no. 5, pp. 443–462, Sep. 1980.
[44] C. Canudas de Wit, H. Olsson, K. J. Astrom, and P. Lischinsky, "A new model for control of systems with friction," *IEEE Trans. Autom. Control*, vol. 40, no. 3, pp. 419–425, Mar. 1995.
[45] M. K. H. Fan, A. L. Tits, and J. C. Doyle, "Robustness in the presence of joint parametric uncertainty and unmodeled dynamics," in *Proc. IEEE Amer. Control Conf.*, Jun. 1988, pp. 1195–1200.
[46] S. R. Moheimani and A. J. Fleming, *Piezoelectric Transducers for Vibration Control and Damping*. London, U.K.: Springer, 2006.
[47] Y. Li, F. Marcassa, R. Horowitz, R. Oboe, and R. Evans, "Track-following control with active vibration damping of a PZT-actuated suspension dual-stage servo system," *J. Dyn. Syst., Meas., Control*, vol. 128, no. 3, pp. 568–576, Sep. 2006.
[48] P.-J. Ko, Y.-P. Wang, and S.-C. Tien, "Inverse-feedforward and robust-feedback control for high-speed operation on piezo-stages," *Int. J. Control*, vol. 86, no. 2, pp. 197–209, Feb. 2013.
[49] K. K. Leang and S. Devasia, "Feedback-linearized inverse feedforward for creep, hysteresis, and vibration compensation in AFM piezoactuators," *IEEE Trans. Control Syst. Technol.*, vol. 15, no. 5, pp. 927–935, Sep. 2007.
[50] Y. Jian, D. Huang, J. Liu, and D. Min, "High-precision tracking of piezoelectric actuator using iterative learning control and direct inverse compensation of hysteresis," *IEEE Trans. Ind. Electron.*, vol. 66, no. 1, pp. 368–377, Jan. 2019.
[51] W. Zhu and X.-T. Rui, "Hysteresis modeling and displacement control of piezoelectric actuators with the frequency-dependent behavior using a generalized Bouc–Wen model," *Precis. Eng.*, vol. 43, pp. 299–307, Jan. 2016.
[52] R. Xu, X. Zhang, H. Guo, and M. Zhou, "Sliding mode tracking control with perturbation estimation for hysteresis nonlinearity of piezo-actuated stages," *IEEE Access*, vol. 6, pp. 30617–30629, 2018.
[53] M. Ming, J. Ling, Z. Feng, and X. Xiao, "A model prediction control design for inverse multiplicative structure based feedforward hysteresis compensation of a piezo nanopositioning stage," *Int. J. Precis. Eng. Manuf.*, vol. 19, no. 11, pp. 1699–1708, Nov. 2018.
[54] Y. Qin and H. Duan, "Single-neuron adaptive hysteresis compensation of piezoelectric actuator based on hebb learning rules," *Micromachines*, vol. 11, no. 1, p. 84, Jan. 2020.
[55] G. Wang, G. Chen, and F. Bai, "High-speed and precision control of a piezoelectric positioner with hysteresis, resonance and disturbance compensation," *Microsyst. Technol.*, vol. 22, no. 10, pp. 2499–2509, Oct. 2016.

IRFAN AHMAD received the M.S. and Ph.D. degrees in control systems from the University of Grenoble (Grenoble Institute of Technology), France, in 2007 and 2011, respectively.

He has worked as a Research and a Teaching Assistant with the GIPSA-Laboratory and Polytech Grenoble, University of Joseph Fourier, Grenoble, France, from 2010 to 2011, and with the Laboratoire de Conception et d'Intégration des Systèmes (LCIS) and ESISAR, Valence, France, from 2011 to 2012. He is currently working as an Assistant Professor with the Department of Electrical Engineering, King Saud University, Riyadh, Saudi Arabia. His current research interests include optimal and robust control design for MEMS/NEMS technology and for other different applications.

MAHMOUD A. ALI received the bachelor's degree in electronic engineering (with specialty of control systems) from the University of Aleppo, Syria, in 2012, and the master's degree in control systems from the Department of Electrical Engineering, King Saud University, Riyadh, Saudi Arabia, in 2019.

In 2018, he has worked as an Assistant Trainer with the Students Center for Creativity and Innovation, King Saud University. His current research interests include optimal and robust control design for micro/nanotechnology, robotics, and switched reluctance motors.

WONSUK KO received the B.S. and M.S. degrees from Kyungwon University, Seongnam, South Korea, in 1996 and 1998, respectively, and the Ph.D. degree in electrical engineering from the University of Central Florida, Orlando, FL, USA, in 2007.

He was a Researcher with the Gachon Energy Research Institute, Gachon University, South Korea, where he was also an Instructor with the Department of Electrical Engineering. He is currently working as an Assistant Professor with the Department of Electrical Engineering, King Saud University, Riyadh, Saudi Arabia. His research interests include electromagnetic modeling, magnetic levitation, energy management, and smart grid.